How to Increase Locking Range of Coupled Oscillator Cells without Lowering Q

Jinjin Shen and L. Wilson Pearson
Department of Electrical and Computer Engineering, Clemson University
Clemson, SC 29634-0915

Abstract — **The locking-range and phase error caused by the random free-running frequency distribution in coupled oscillator phased arrays are studied. A design method on coupling optimization is proposed to improve the oscillator locking-range and thereby reduce the phase error. A qualitative analysis and experimental results are presented to demonstrate the viability of this method for improving the fabrication tolerance of coupled oscillator phased arrays.**

I. Introduction

The coupled oscillator phased arrays have been proposed as a means for beam-steering without phase shifters. In a coupled oscillator array, a phase progression is generated through the control of the free-running frequency or phase of the perimeter elements in the array [1-7].

The steady-state phase dynamics of a one-dimensional array with N coupled oscillators can be described by equations

$$\begin{aligned}\omega_0 &= \omega_1 - \frac{\omega_1 \kappa}{2Q}\cdot\sin(\Phi+\theta_1-\theta_2)\\ \omega_0 &= \omega_i - \frac{\omega_i \kappa}{2Q}\cdot[\sin(\Phi+\theta_i-\theta_{i-1})\\ &\quad +\sin(\Phi+\theta_i-\theta_{i+1})]\\ \omega_0 &= \omega_N - \frac{\omega_N \kappa}{2Q}\cdot\sin(\Phi+\theta_N-\theta_{N-1})\end{aligned}, \qquad (1)$$

where θ is the instantaneous phase of each oscillator, ω_i is the free-running frequency of the ith oscillator, ω_0 is the ensemble frequency of the mutually locked oscillator array, κ and Φ are the coupling strength and phase between adjacent oscillators, respectively, and Q is the quality factor of the resonant circuit for each oscillator, and $2 \le i \le N-1$.

In the set of equations (1), difference between the oscillator free-running frequency and array ensemble frequency is compensated by the phase-shift between adjacent elements. Because fabrication differences inevitably result in random fluctuation on free-running frequencies, the phase difference terms in the sine functions have to take on corresponding random values to satisfy the equations in (1). In this way, random fluctuations in the free-running frequency, which arise through fabrication differences, are translated into phase errors across the phase front of the array.

It is desirable to minimize these phase errors. First of all, one would seek to make the free-running frequencies agree as tightly as possible. At short wavelengths, one is quite likely to resort to integrated fabrication and packaging of the circuitry associated with the array of oscillators. This makes it difficult to do any trimming on individual elements in order to adjust the oscillator free-running frequencies. As a solution, a post-fabrication calibration technique is proposed in [8] to reduce the influence of phase errors, without resorting to much circuit adjustment. The second recourse to control the occurrence of phase error is to maximize the factor $\omega_i\kappa/2Q$ appearing in the expressions, which is also familiar to people as the locking-range of oscillator. This heightens the sensitivity of the equations to phase difference, so that little phase difference is required to bring the equations into agreement in the presence of frequency differences. This choice reduces the sensitivity of intended beam steering to frequency change, therefore applied frequency differences for a given steering angle must be relatively large. In following sections, a design method to increase oscillator locking-range is analyzed.

II. Locking-range and Oscillator Equivalent Circuits

Shown in (1), the locking-range is controlled by the oscillator quality factor Q and inter-element coupling strength κ, which are described in [2]. If we express Q and κ in terms of the circuit parameters in the oscillator equivalent circuit and array coupling network, we can rewrite the locking-range expression as

0-7803-7239-5/02/$10.00 © 2002 IEEE

$$\frac{\omega_i \kappa}{2Q} = \begin{cases} \dfrac{R_L^2}{4Z_0 L} & \text{for series-resonant circuit} \\ \dfrac{1}{4Z_0 C} & \text{for shunt-resonant circuit} \end{cases}, \quad (2)$$

where L, C, R_L are the components in the oscillator equivalent circuits, shown in Fig. 1, and Z_0 is the array coupling resistance described in [2].

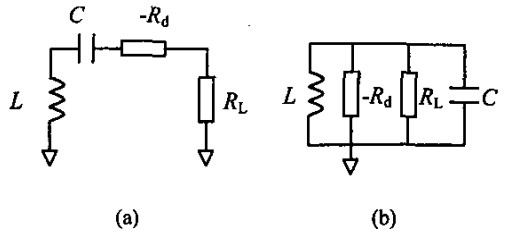

Fig. 1 Oscillator Equivalent Circuit: (a) Series-Resonance, (b) Shunt-Resonance

With the equation (2), we can predict and optimize the oscillator locking-range qualitatively in order to reduce phase error.

A solution to maximize the factor $\omega_i\kappa/2Q$ in equations (1) is to lower Q [9]. But the undesirable effect of a low Q oscillator is its higher phase noise. This poses question of how to manage the degraded phase noise in low-Q oscillator arrays. To avoid this problem, we consider the equation (2), which is equivalent to the equation (1). An oscillator can be approximated with *RLC* equivalent circuit acting in tandem with a negative resistance element, $-R_d$. The circuit can be either series-resonant or shunt-resonant, as shown in Fig. 1. A lower value of C increases the locking-range for the shunt-resonant circuit directly as one may observe from (2). A reduction in C coupled with an increase in R_L may increase locking range for the series case. These changes also change the quality factors Q of both circuits. However, the definition of Q reminds us that it's possible to reduce C without significantly lower the Q factor by adjusting R_L at the same time. By focusing on the adjustment of circuit elements directly, rather than on κ and Q, we can increase the locking range without reducing Q.

Fig. 2 shows the schematic for an oscillator design. The capacitor at the source lead provides the positive feedback for oscillation, and the inductor at the gate lead resonates with the capacitive gate impedance. The drain lead is connected to a resistive load. A small-signal equivalent-circuit model for the Fujitsu FHX35LG HEMT was used in the simulation. Proper simulations, for either input impedance or input admittance, are performed for all three ports to represent their resonance properties. The simulation results over the frequency range of 9 GHz to 11 GHz are shown in Fig. 4, 5, and 6. One can discern from the slope of the imaginary parts on the immitances plots for Y_G, Y_S, and Z_D, that the drain port shows a series-resonance, and both the source port and gate port show a shunt-resonance. The comparison of Fig. 4 and 5 shows that the slope of the imaginary part of the gate input admittance is less steep than that of the source input admittance. This means the equivalent capacitance at the gate port is smaller than that at the source port, and thereby may result in a larger oscillator locking range when coupling at the gate ports, according to the equation (2), while the oscillator Q factor remains the same.

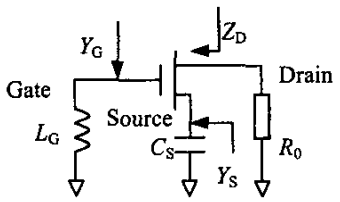

Fig. 2 Oscillator Schematic

III. Experimental Results

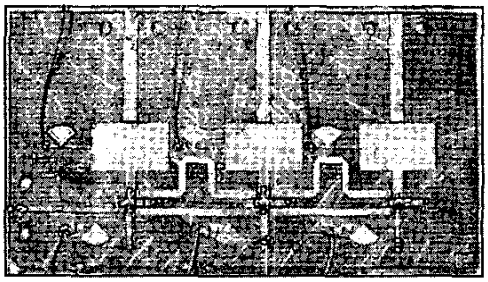

Fig. 3 Coupled oscillator array with 3 elements

A 3-unit VCO array, shown in Fig. 3, is built to experimentally test the design method. Each VCO is designed based on the oscillator topology in Fig. 2 and includes a Fujitsu FHX35LG HEMT loaded with a microstrip patch antenna at its drain port. The antenna array has a center-to-center spacing of $0.8\lambda_0$. The free-running frequency of oscillators can be tuned by changing the DC biases on varactors. First, each oscillator was tuned approximately to have a free-running frequency of 9.9 GHz. Then they were mutually coupled to their nearest neighbors. Three successive

measurements were performed, each with a different coupling format: coupling between drain ports with a one-wavelength microstrip line, coupling between gate ports with a one-wavelength microstrip line and coupling between source-port with a half-wavelength microstrip line. Two 43 Ω chip resistors were inserted at the ends of each coupling line.

We observed the oscillator locking-range for the respective cases by pushing the scan range of the oscillator array until locking became broken. Table 1 shows the beam-steering measurement results of the oscillator array for the three cases. The radiation patterns are displayed in Fig. 7, 8, and 9. The theoretical beam scanning range of the array is [-18.2°, +18.2°], based on the array period. In all three measurements the beam could be steered over a substantial fraction of the theoretical limits. In the case of source coupling, the oscillators broke lock at ± 50 MHz detuning of the end elements. In the case of drain coupling, the array could be detuned to ± 300 MHz before lock was broken, with concomitantly (but not proportionately) larger beam steering range. With the gate coupling, even ± 400 MHz did not break lock among the oscillators. However, the phase scanning saturate at nearly the theoretical limit for this detuning.

The experiments demonstrated that greater locking-ranges were obtained through a coupling optimization without lowering the oscillator Q factor. With the relatively large locking-ranges, the beam-steering ranges from the gate and drain couplings are rather similar and symmetrical. But with a small locking range, the source-coupling setup shows an asymmetrical beam-steering affected by the phase error in the oscillator array.

IV. Conclusions

With refined oscillator circuit design and optimization of inter-element coupling, a larger locking range for coupled oscillator array can be obtained without resorting to lower the Q factor of individual oscillators. The different locking-ranges shown in three cases can be explained with the equivalent circuits of the three ports and the associated capacitance interpretations. This helps to reduce the random phase error caused by fabrication difference in coupled oscillator arrays.

Acknowledgement

This work was sponsored by a DoD MURI Program, "Spatial and Quasi-Optical Power Combining," under Contract Number DAAG55-97-1-0132.

References

1. P. Liao and R.A. York, "A new phase-shifterless beam-scanning technique using arrays of coupled oscillators," *IEEE Trans. Microwave Theory and Tech.*, Vol. MTT-41, No.10, pp1810-1815, Oct.1993
2. R. A. York, P. Liao, and J. J. Lynch, "Oscillator Array Dynamics with Broadband N-Port Coupling Networks", *IEEE Trans. Microwave Theory and Tech.*, vol. 42, pp. 2040-2045, Nov. 1994
3. H. C. Chang, E. S. Shapiro and R. A. York, "Influence of the oscillator equivalent circuit on the stable modes of parallel-coupled oscillators," *IEEE Trans. Microwave Theory and Tech.*, Vol. MTT-45, No.8, pp1232-1239, Aug.1997
4. L. Wilson Pearson and Ronald J. Pogorzelski, "A Fresh Look at Spatial Power Combining Oscillators," *National Radio Science Meeting*, Boulder, CO, January 1999.
5. R. J. Pogorzelski, P. F. Maccarini, and R. A. York, "A Continuum Model of the Dynamics of Coupled Oscillator Arrays for Phase-Shifterless Beam Scanning," *IEEE Trans. Microwave Theory and Tech.*, Vol. 47, No. 4, pp463-470, April, 1999
6. R. J. Pogorzelski, P. F. Maccarini, and R. A. York, "Continuum Modeling of the Dynamics of Externally Injection-Locked Coupled Oscillator Arrays," *IEEE Trans. Microwave Theory and Tech.*, Vol. 47, No. 4, pp. 471-478, April, 1999
7. L. W. Pearson and J. Shen, "Coupled-Oscillator Spatial Power Combining," *XXVth General Assembly of the International Radio Science Union*, Montreal, CA, August, 1999
8. J. Shen and L.W. Pearson, "Oscillator Reproducibility Consideration in Coupled Oscillator Phase-steering Arrays", *IEEE International Microwave Symposium*, Boston, MA, June, 2000
9. L.W. Pearson, J. Shen and C.M. Tompkins, "Coupled-Oscillator Arrays: Beamsteering without Phase Shifters", *IEEE International Symposium on Phased Array Systems and Technology*, Dana Point, CA, May, 2000

Table 1 Beam-steering ranges with different VCO couplings

Coupling Scheme	Frequency Tuning (MHz)	Scanning Range (degrees)
Gate Coupling	± 400	(-17°, +16°)
Drain Coupling	± 300	(-17°, +15°)
Source Coupling	± 50	(-8°, +20°)

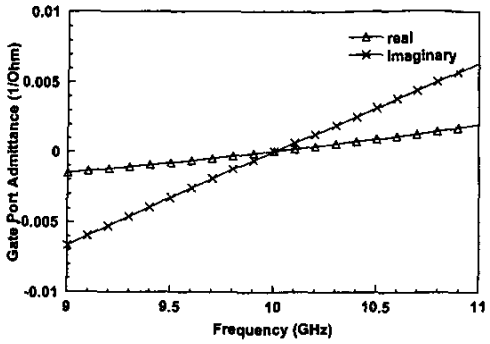

Fig. 4 Simulation of the Input Admittance at Gate

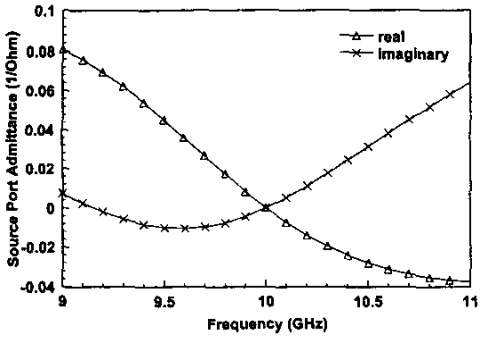

Fig. 5 Simulation of the Input Admittance at Source

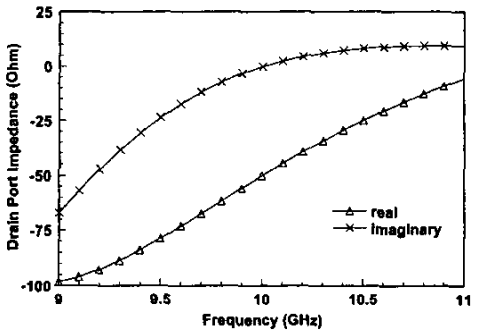

Fig. 6 Simulation of the Input Impedance at Drain

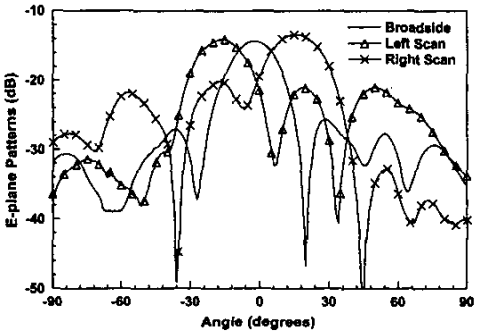

Fig. 7 Measured Radiation Patterns of Gate Coupling

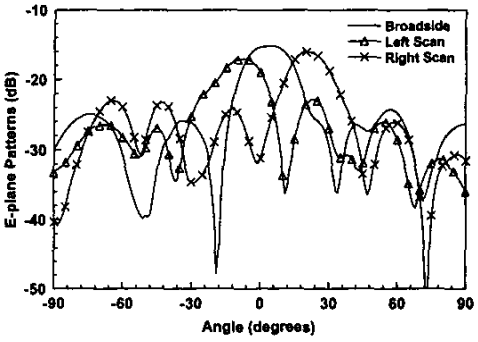

Fig. 8 Measured Radiation Patterns of Source Coupling

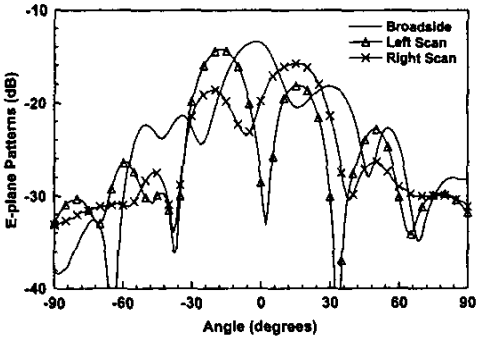

Fig. 9 Measured Radiation Patterns of Drain Coupling